Article No. jmbi.1998.2445 available online at http://www.idealibrary.com on IDEAL J. Mol. Biol. (1999) 286, 267–278

JMB

Enzyme Specificity Under Dynamic Control: A Normal Mode Analysis of α-Lytic Protease

David W. Miller and David A. Agard*

Howard Hughes Medical Institute and Department of Biochemistry and Biophysics University of California at San Francisco, San Francisco CA 94143-0448, USA

**Corresponding author*

We have used α-lytic protease as a model system for exploring the relationship between the internal dynamics of an enzyme and its substrate specificity. The wild-type enzyme is highly specific for small substrates in its primary specificity pocket, while the M190A mutant has a much broader specificity, efficiently catalyzing cleavage of both large and small substrates. Normal modes have been calculated for both the wild-type and the mutant enzyme to determine how internal vibrations contribute to these contrasting specificity profiles. We find that for the atoms lining the walls of the specificity pocket, the wild-type normal modes have a more symmetric character, with the walls vibrating in phase, and the size of the pocket remaining relatively fixed. This is in agreement with X-ray crystallographic data on conformational substates trapped at 120 K. In contrast, we find that in the mutant, the binding pocket normal modes have a more antisymmetric character, with the walls vibrating out of phase, and the pocket able to expand and contract. These results suggest that the internal vibrations of a molecule may play an important role in determining substrate binding and specificity. A small change in protein structure can have a significant effect on the pattern of molecular vibrations, and thus on enzymatic properties, even if the overall amplitudes of the vibrations, as measured by NMR relaxation or crystallographic *B*-factors, remain largely unchanged.

Keywords: normal mode analysis; enzyme specificity; α-lytic protease; protein dynamics; protein mutagenesis

Introduction

The primary function of an enzyme is to catalyze chemical reactions by binding substrates in a manner that stabilizes the reaction transition state (Pauling, 1948). A hallmark of biological enzymes is that they can distinguish between many different substrates and can selectively catalyze only those reactions appropriate for a particular function. The molecular basis for such substrate specificity is in large part determined by the detailed shape of the enzyme active site: those substrates having transition-state conformations complementary to the enzyme surface may bind and undergo catalysis, while those resulting in less favorable interactions are catalyzed at lower rates or are not catalyzed at all.

This structural basis for enzyme specificity has been well established by experiments combining mutational analysis and X-ray crystallographic structure determination: transition-state stabilization appears to occur through a complex balance between favorable (e.g. hydrogen bonding, electrostatic complementarity and burial of hydrophobic surfaces) and unfavorable (e.g. bond distortion, cavity formation and entropic penalties) interactions in the enzyme-substrate complex. However, it is not well understood what role dynamics may play in specificity. Although various types of motions in proteins are clearly important for ligand binding (see Discussion), such motions are typically used to regulate the movement of substrates and products into and out of the active site, or of small molecules into the protein interior, and are not normally considered necessary for discrimination between various different substrates. Is it possible that dynamics may also play a role in

Present address: D. W. Miller, CombiChem, 1804 Embarcadero Road, Suite 201, Palo Alto, CA 94303, USA.

Abbreviations used: αLP, α-lytic protease; NMA, normal mode analysis; pNA, *p*-nitroanilide; sAAP, succinyl-L-Ala-L-Ala-L-Pro-.

E-mail address of the corresponding author: agard@msg.ucsf.edu

0022-2836/99/060267–12 $30.00/0

selecting one particular substrate while excluding others that may be similar?

α-Lytic protease (αLP) represents an excellent model system for exploring the molecular basis of enzyme specificity. An extracellular serine protease of the bacterium *Lysobacter enzymogenes* that is structurally homologous to mammalian serine proteases of the trypsin family (Brayer *et al*., 1979), αLP is specific for substrates having small hydrophobic side-chains at the P_1† position. High-resolution crystal structures have been obtained of αLP alone and in complex with various covalently bound peptide transition-state analogs, and show that the hydrophobic P_1 side-chain is buried in the complementary S_1 pocket of the enzyme (Bone *et al*., 1987, 1989b, 1991; Figure 1).

In wild-type form, αLP has a narrow specificity profile: in the catalysis of succinyl-Ala-Ala-Pro-X-*p*-nitroaniline (sAAPX-pNA) substrates, where X is the P_1 residue, αLP shows a strong preference for Ala at P_1 over larger hydrophobic side-chains, in k_{cat}/K_M values and in K_i values for the analogous peptide inhibitors (Bone *et al*., 1989a,b; 1991; Figure 2). However, when a Met residue in the active site is mutated to Ala (M190A‡), the specificity profile is considerably broadened: large values of k_{cat}/K_M are observed for all P_1 residues, and the distribution of rates is much more uniform than in the wild-type enzyme. Particularly striking is the difference in catalytic rates between the Ala and Phe substrates: whereas in the wild-type enzyme this difference is more than four orders of magnitude, in the mutant it is only around one (Figure 2). Changes in k_{cat}/K_M values are shown to result largely from changes in K_M, while k_{cat} remains relatively constant (Bone *et al*., 1989a).

A large reason for the observed broadening in specificity is structural: Met190 partially fills the S_1 active-site pocket and prevents side-chains larger than Ala from binding in optimal orientations (Bone *et al*., 1989a, 1991). Yet there is evidence that the broadening may also be influenced by structural plasticity. First, the specificity profile for M190A is remarkably different from chymotrypsin, an enzyme that has a large, rigid hydrophobic pocket and displays very poor catalysis of small hydrophobic substrates (Wallace *et al*., 1963). Secondly, in complexes of the mutant with different peptide inhibitors, the S_1 pocket shows expansion for larger substrates and contraction for smaller ones, relative to the unbound state, whereas the equivalent complexes in the wild-type show relatively little plasticity (Bone *et al*., 1989a,b, 1991). A third piece of evidence is provided by a low-temperature crystal structure of wild-type αLP at 120 K (Rader & Agard, 1997). At such low temperatures, thermal fluctuations are effectively eliminated, and regions of elevated crystallographic *B*-factors are considered to be the consequence of trapped conformational substates. These substates were analyzed by fitting the electron density with a set of structures (Burling *et al*., 1996), while maintaining a fixed *B*-factor (Rader & Agard, 1997). The structures indicate that the walls of the binding pocket must be able to sample multiple conformations at room temperature, and further suggest that the strands that form the S_1 pocket move in a cooperative or ''symmetric'' manner, such that the interior dimensions of the pocket remain fixed.

These results suggest that in addition to structure, molecular vibrations may play a significant role in αLP specificity. In particular, the low-temperature data suggest the hypothesis that whereas the wild-type S_1 pocket shows symmetric motion which conserves the size of the binding pocket and consequently narrows the specificity profile, the S_1 pocket of the M190A mutant might exhibit increased antisymmetric motion, allowing the pocket to expand and contract, significantly broadening the specificity by allowing P_1 residues of varying size to bind in the pocket and undergo catalysis.

To test this hypothesis and to determine the extent to which dynamics influences the two

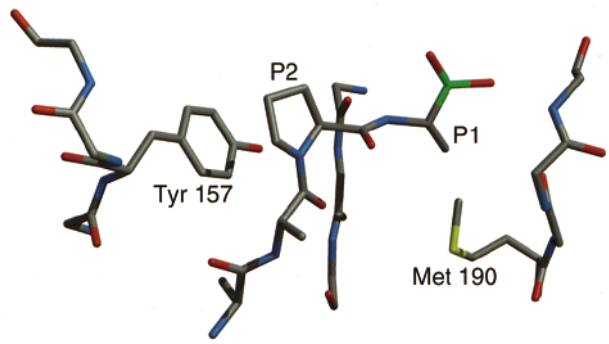

Figure 1. The primary (S_1) and secondary (S_2) specificity pockets of α-lytic protease bound with the inhibitor methoxysuccinyl-Ala-Ala-Pro-Ala Boronic acid. The P_1 Ala side-chain of the inhibitor inserts between the two protein segments (Met190-Gly191-Arg192-Gly193 and Ser214-Gly215-Gly216) that form the walls of the S_1 pocket. The P_2 Pro side-chain packs against Tyr157 of the methionine loop, which forms part of the S_2 pocket. The Figure shows only main-chain atoms of the protein (except Tyr157 and Met190, which forms the base of the S_1 pocket), and all atoms of the ligand. Coordinates were taken from the structure indexed 1p02 in the PDB. All molecular graphics images were produced using the MidasPlus program (Ferrin *et al*., 1988; Huang *et al*., 1991) from the Computer Graphics Laboratory, University of California, San Francisco.

† The P and S nomenclature by Schechter & Berger (1967) is used. P_1 is the substrate residue before the scissile bond; P_2, P_3, etc. extend toward the N terminus. S_1, S_2, etc. are the corresponding binding subsites on the enzyme.

‡ Residues are numbered according to the system described by Fujinaga *et al*. (1985) and reflect structural homology with chymotrypsin. Several earlier papers from the Agard Lab used a slightly different numbering scheme (James *et al*., 1978). For reference, Met192 in the old scheme becomes 190.

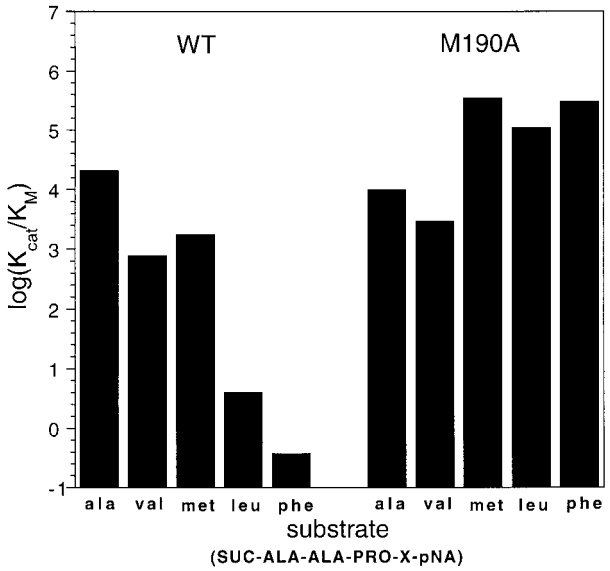

Figure 2. The effect of mutations on specificity. Log(k_{cat}/K_M) is shown as a bar for each of five substrates, sAAP-X-pNa, where X = Ala, Val, Met, Leu, and Phe, for the wild-type enzyme and mutant M190A. (Data from Bone *et al.*, 1989a,b; 1991.)

characteristic specificity profiles, we have used normal mode analysis (NMA) to calculate the internal molecular vibrations of αLP in its wild-type and mutant forms. The method, which approximates all the individual vibrational states of a molecule, is described in detail below. For validation, we calculate expected *B*-factors from the normal mode data, and compare them with the actual *B*-factors derived from X-ray crystallography. We then explore how the normal mode-derived vibrations affect the structure of the S_1 specificity pocket, both for wild-type and mutant αLP, and discuss the results in light of the known specificity profiles.

Normal Mode Analysis

Normal mode analysis provides an approximation to the atomic motion of a molecule by dividing it into its vibrational components (for a review, see Case, 1994). Long used to study small-molecule vibrations, NMA has only recently become a computationally tractable method for studying large systems such as proteins (Brooks & Karplus, 1983; Go *et al.*, 1983; Levitt *et al.*, 1985). It is now routine to perform calculations on systems consisting of hundreds or even thousands of atoms. Recent applications of NMA to proteins have included the mapping of energy landscapes (Hayward *et al.*, 1994, 1995); analyzing the energetics of large-scale conformational changes (e.g. Gibrat & Go, 1990; Tirion & ben-Avraham, 1993; Marques & Sanejouand, 1995; Sanejouand, 1996; Mouawad & Perahia, 1996); estimating configurational entropies (Karplus & Kushick, 1981; Levy *et al.*, 1984; Tidor & Karplus, 1993); and refining crystallographic *B*-factors (Diamond, 1990; Kidera & Go, 1992; Kidera *et al.*, 1992).

Here, we extend the use of the NMA method by applying it to two new and important problems: (1) the effects of a point mutation on internal protein dynamics, and (2) the influence of molecular vibrations on enzyme specificity. The implications of our results are considered at length in the Discussion. Below we give a brief summary of the NMA technique, and outline some of the benefits and limitations associated with the method.

Assuming each atom in an *N*-atom system moves in a harmonic potential, the equation of motion, $\vec{x}$, for the 3*N* atomic degrees of freedom is given by:

$$Fx = \omega^2 M\bar{x} \tag{1}$$

where *F* is the 3*N*-by-3*N* force-constant matrix, $F_{ij} = \delta^2 E/\delta x_i \delta x_j$; *M* is the diagonal matrix of atomic masses; and ω is the frequency of harmonic motion. Equation (1) can also be written in terms of the Hessian matrix *H*:

$$H\bar{q} = \omega^2\bar{q} \tag{2}$$

where $H = M^{-1/2}FM^{-1/2}$ is the mass-weighted force-constant matrix, and $\vec{q} = M^{1/2}\vec{x}$ is the mass-weighted Cartesian displacement vector.

The full solution to equation (2) is a set (designated *Q*) of 3*N* vectors $\vec{q}$, and their 3*N* associated frequencies, such that *Q* and the ω_i satisfy:

$$HQ = Q\text{diag}(\omega_1^2, \omega_2^2, \ldots, \omega_{3N}^2) \tag{3}$$

$$Q^{-1}HQ = \text{diag}(\omega_1^2, \omega_2^2, \ldots, \omega_{3N}^2) \tag{4}$$

The solution is thus obtained by diagonalization of the Hessian matrix *H*. The 3*N* eigenvectors (normal modes) are the columns of the transformation matrix *Q*, and the 3*N* eigenvalues (squared frequencies) are the diagonal elements of the diagonalized matrix diag(ω_1^2, ω_2^2, ... ,.ω_{3N}^2).

There are three main disadvantages of normal mode analysis as compared with all-atom simulation techniques. First, the method assumes that motion is harmonic in each degree of freedom. This assumption has been shown to introduce significant errors in some model systems (Ichiye & Karplus, 1991; Hayward *et al.*, 1994, 1995), although comparisons of normal modes with molecular dynamics (MD) simulations have in general shown at least qualitative agreement (Teeter & Case, 1990; Hayward *et al.*, 1994, 1995). Second, computer memory limitations often restrict the number of atoms and the number of degrees of freedom that can be represented. Energy calculations are thus performed *in vacuo*, and the protein representation is usually simplified, for example by modeling only polar hydrogen atoms. Recently several new methods have been developed to selectively obtain only partial normal mode information, resulting in a significant reduction in computational expense (Hao & Harvey, 1992, 1994;

Mouawad & Perahia, 1993; Durand *et al.*, 1994). Third, normal mode calculations involve expansion about a single minimum on the energy landscape, so they neglect any contributions to dynamics which may arise from transitions between energy minima. The expected contributions of such transitions to overall dynamics remain a source of debate (see Thomas *et al.*, 1993; Case, 1994; Hayward *et al.*, 1994, 1995).

Yet despite these limitations, NMA offers several advantages over the all-atom methods. First, it allows complex motion to be reduced to its simplest components, such as large-scale hinge bending. Such a reduction greatly simplifies the analysis of dynamics, especially since only a small number of low-frequency modes make significant contributions to the overall motion (see Methods). Second, the method is computationally straight forward. Unlike MD simulations, NMA can provide information about low-frequency motions without the need to calculate long trajectories. Lastly, and perhaps most importantly, NMA provides a rigorous connection between the dynamic picture of the protein and the energetic one. Since vibrations are calculated at a single minimum in the energy landscape and neglect barrier crossing, the modes of low-frequency motion will reveal the directions along which the energy minimum is most shallow. In other words, the directions of low-frequency vibration should also correspond with the directions of significant structural plasticity. This feature of connecting dynamics with thermodynamics increases the power of NMA to model important functional aspects of the protein, such as the energetics of ligand binding.

Despite its limitations, NMA has been shown to provide a surprisingly accurate description of the large-scale, functionally important motions in many different proteins, including hemoglobin (Mouawad & Perahia, 1996), lysozyme (Brooks & Karplus, 1985; Gibrat & Go, 1990; Horiuchi & Go, 1991; Mouawad & Perahia, 1993), citrate synthase (Ech-Cherif El-Kettani & Durup, 1992; Marques & Sanejouand, 1995), and hexokinase (Harrison, 1984). We therefore consider the method to be a useful starting point for elucidating basic principles governing the relationship between protein dynamics and function.

Results

Normal modes were calculated for the wild-type αLP and the M190A mutant, both as free enzymes and as complexes with the peptide transition-state inhibitor MeO-suc-Ala-Ala-Pro-BoroAla using previously determined high-resolution X-ray structures (Fujinaga *et al.*, 1985; Bone *et al.*, 1989b; Mace & Agard, 1995; Mace *et al.*, 1995). Figure 3 shows the distribution of normal modes for the unliganded wild-type αLP, obtained from diagonalization of the Hessian matrix. (The mutant modes have a nearly identical distribution and are not shown.) Of the 5274 modes, the first six correspond with translational and rotational motion and have zero frequency. The non-zero modes range in frequency from 3.35 cm^{-1} to 3744.59 cm^{-1}, corresponding with a vibrational time-scale of tens to hundredths of picoseconds. The shape of the distribution, with a peak in the low-frequency region, is similar to those reported for other proteins (e.g. Levitt *et al.*, 1985; Brooks & Karplus, 1983; Gibrat & Go, 1990; Tiron & ben-Avraham, 1993).

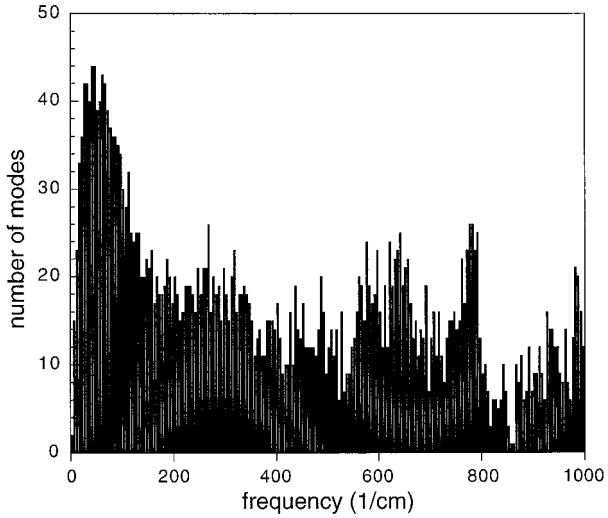

Figure 3. The distribution of normal modes for wild-type αLP. The histogram shows the mode density *versus* frequency for all normal modes less than 1000 cm^{-1}. The bin width is 5 cm^{-1}.

Figure 4 shows residue *B*-factors for wild-type αLP. The lower trace shows *B*-factors obtained from X-ray crystallography (2alp; Fujinaga *et al.*, 1985), while the upper trace shows theoretical *B*-factors calculated from the wild-type normal modes (see Methods). The two curves are qualitatively quite similar, showing elevated motions (peaks in the *B*-factors) in the same protein regions, and they display a level of agreement similar to what has been observed in other protein systems (Levitt *et al.*, 1985; Gibrat & Go, 1990; Tiron & ben-Avraham, 1993). *B*-factors for the mutant protein, both calculated and crystallographic, show only minor differences from the wild-type values (Bone *et al.*, 1989a), and are not shown.

Although there are quantitative differences in the predicted motions, some of these may be due to non-vibrational components of the crystallographic *B*-factors, such as static disorder and anisotropic motion (see Daggett & Levitt, 1993), or to the effects of crystal contacts. As an example of the latter effect, the loop containing residue 83, for which NMA appears to highly over-predict the dynamics, is involved in a crystal contact and so may have crystallographic *B*-factors that considerably underestimate its motion in solution. In a different crystal structure of αLP in complex with its Pro region, the same loop does not make such a

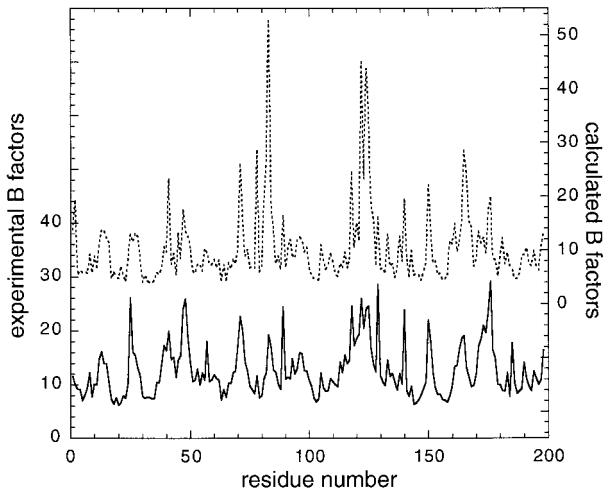

Figure 4. Residue *B*-factors for wild-type αLP. The lower trace shows crystallographic *B*-factors, and the upper trace shows equivalent *B*-factors derived from the normal modes (see Methods). The amino acid numbering on the *x*-axis is sequential notation, so the S_1 pocket strands in Figure 1 become Met138-Gly141 and Ser159-Gly161. The *y*-axis numbering to the right of the Figure applies to the normal-mode data.

contact and has a considerably higher *B*-factor, much closer to what is predicted by NMA (Sauter *et al.*, 1998). While close quantitative comparisons of experimental and theoretical *B*-factor values remain difficult, it appears that many of the general features of αLP dynamics are captured by the normal mode results.

The S_1 pocket

To investigate whether or not the calculated normal mode vibrations are consistent with the specificity profiles of wild-type and mutant αLP, we have analyzed the predicted motions of the atoms lining the walls of the S_1 specificity pocket. We first define a group of 25 "specificity atoms," which satisfy the two requirements that they be in one of the two walls of the S_1 pocket (the Met190-Gly193 strand or the Ser214-Gly216 strand; see Figure 1), and that they be in close contact with the P_1-residue side-chain of the inhibitor. We have arbitrarily chosen a cutoff distance of 5 Å from the C^{β} of the P_1 side-chain.

Using these calculations, we then ask: are the cavity walls predicted to vibrate symmetrically, or are they predicted to vibrate antisymmetrically? In other words, do the two wall-forming strands move in unison, such that the size of the S_1 pocket remains unchanged, or do they move in opposite directions, such that the pocket expands and contracts as the strands vibrate? To answer this question, we define two sets of vectors, corresponding with symmetric and antisymmetric motion, respectively. Each set consists of 25 three-dimensional vectors, one for each of the specificity atoms defined above. The vectors are of constant arbitrary length, but the directions are such that in the symmetric set, the pocket walls move in the same direction, while in the antisymmetric set they move in opposite directions. Figure 5(a) shows a sample of ten vectors from a set of 25 used to represent symmetric motion. The set of antisymmetric vectors is identical, except that the vectors of one of the two strands have the opposite sign. Each of these two vector sets now comprises a multidimensional "difference vector," whose dot product with any one of the calculated normal modes is a quantitative measure of how much symmetry

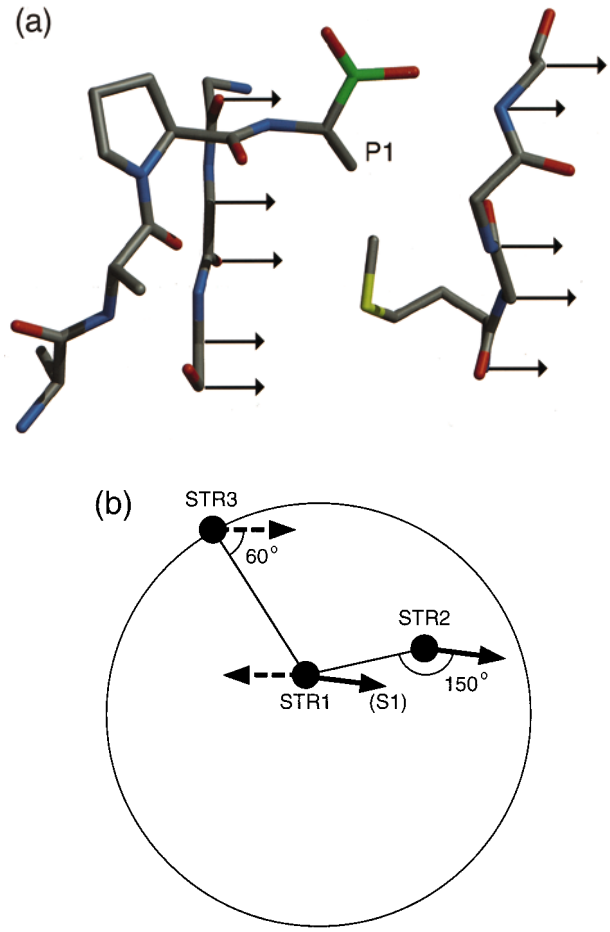

Figure 5. (a) Diagram illustrating the difference vector used to represent symmetric motion of the two S_1 pocket chain segments. Ten sample vectors are shown (see the text and the Methods). (b) Schematic illustration of the method used to calculate the angular dependence of vibrations. The Figure depicts α-lytic protease oriented such that the axis of each of the three protein strands of interest points into the page. STR1 and STR2 (Ser214-Gly216 and Met190-Gly193, respectively) are the strands that form the S_1 pocket, while STR3 and STR1 (the former being residues Tyr171-Gly174 of the methionine loop) form the S_2 pocket. The continuous arrows show symmetric motion of the S_1 pocket, while the broken arrows show antisymmetric motion of the S_2 pocket. The Figure illustrates how the vibration angle is measured with respect to a principal axis.

or antisymmetry is present in that particular mode. (Further details are provided in Methods.)

The results of these calculations for the 100 lowest-frequency normal modes of both the wild-type and mutant αLP are shown in Figure 6(a) and (b). In the wild-type enzyme (Figure 6(a)), the symmetric vibrational motion has a much larger amplitude than the antisymmetric motion in the region of the S_1 pocket. In contrast, in the mutant enzyme (Figure 6(b)), the antisymmetric motion has become considerably stronger relative to the wild-type value, and the symmetric motion has become weaker, with the result that the two types of motion have approximately similar amplitudes. Calculations indicate that the root-mean-square displacement of the antisymmetric vibrations (equation (5)) increases nearly twofold, from approximately 0.3 Å to 0.6 Å following mutation (Figure 6(a) and (b)).

These results appear consistent with the observed specificity profiles for the wild-type and mutant enzymes. In the case of wild-type αLP, normal-mode vibrations in the binding pocket tend to be such that the interior dimensions of the pocket are preserved. This suggests a structural rigidity that may be a factor in preventing P_1 side-chains larger than Ala from binding favorably within the cavity. On the other hand, when the binding-site Met is mutated to Ala, the vibrational modes are altered such that the pocket is allowed more freedom in opening and closing. The contribution from the antisymmetric component alone would allow changes in the pocket size in excess of 1.2 Å. While the precise magnitude of the fluctuations are

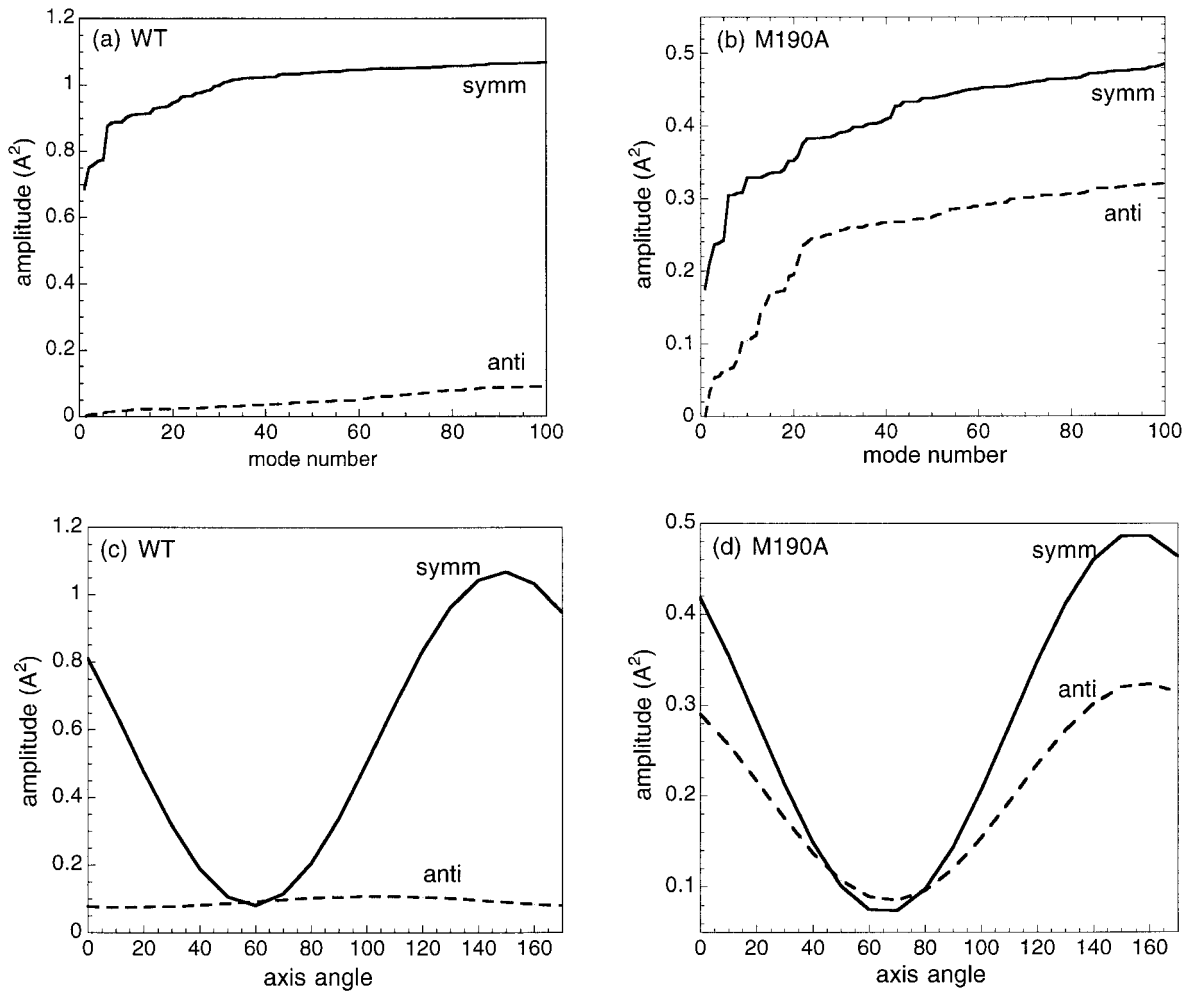

Figure 6. (a) and (b) Dot product calculations. The *x*-axis is the mode number for the 100 lowest-frequency modes. The *y*-axis (amplitude) is the cumulative squared dot product between each normal mode and the multi-dimensional vector representing motion of the S_1 pocket in either a symmetric or antisymmetric direction (magnitudes calculated at room temperature from equation (5). The wild-type normal modes (a) show only symmetric motion, while the mutant modes (b) show both symmetric and antisymmetric motion. Calculations are for 25 atoms that form the walls of the S_1 pocket, as explained in the text and the Methods. (c), (d) Angular variations. The cumulative squared dot product after 100 modes (amplitude) from (a) and (b) is plotted *versus* the angle of the vibrational axis (see Methods). Both symmetric (continuous line) and antisymmetric (broken line) motions in the mutant (d) occur along the same optimal axis, which is also the optimal axis for the symmetric motion in the wild-type (c). Antisymmetric motion in the wild-type occurs along an orthogonal axis. Figure 5(b) illustrates how the optimal axis is oriented with respect to the αLP structure.

uncertain due approximations inherent in the NMA method, the dramatic change in the vibrational profile suggests a direct contribution of dynamics to the mutant's ability to accommodate both large and small side chains.

If the preceding view is correct, then there should be a clear angular dependence to the motion, with the dominant axis being well correlated with opening and contracting the binding pocket. To test this hypothesis, we performed an analysis of the angular behavior of the symmetric and antisymmetric motions. All vectors were collectively rotated about an imaginary axis running parallel with the two protein strands, and dot product calculations were performed at discrete angles. By convention, we have chosen 0° tilt to be parallel with the vector joining the two β-sheet strands (Figure 5(b)). Results of the angular variation indicate that for the mutant enzyme (Figure 6(d)), both the symmetric and antisymmetric types of motion have the same ''optimal'' axis, corresponding with the direction of maximum vibrational amplitude. For the wild-type enzyme (Figure 6(c)), symmetric motion has the same optimal axis as in the mutant, while the very low-amplitude antisymmetric motion has an optimal axis that is roughly orthogonal to the symmetric axis. Figure 5(b) shows schematically how this optimal axis angle of 150° in Figure 6(c) and (d) relates to the αLP structure, and verifies that this value gives a good approximate description for opening and closing of the S_1 pocket.

In addition to the cumulative data of Figure 6, the calculated vibrational modes also appear to support our hypothesis on an individual basis. Figure 7 shows two examples of individual low-frequency modes (the lowest-frequency mode of wild-type αLP and the mode of second-lowest frequency for the mutant), which exhibit symmetric and antisymmetric motion, respectively. In the wild-type, the two wall-forming strands move in unison, largely preserving the size of the pocket, and closely resembling the results of the multiple-structure refinement at low temperature (Rader & Agard, 1997). Conversely, in the mutant the strands close in on one another, making the pocket smaller. Although many of the low-frequency modes in both the wild-type and mutant show motion that is more complex than the simple opening and closing described in Figures 5-7 (for example, the lowest mode of the mutant actually shows significantly symmetric motion), it is evident by inspection that a much larger fraction of the mutant modes show at least some degree of plasticity in the S_1 pocket, while in the wild-type the pocket is considerably more rigid.

A structural basis for this vibrational difference is suggested from the X-ray crystal structures of the wild-type and the M190A mutant. Replacing Met with Ala creates a gap in the van der Waals packing at the base of the S_1 pocket (data not shown), the result of which may be to introduce a new degree of freedom into the local vibrations, thus reducing the rigidity of the S_1 pocket by allowing it to expand and contract. If such reasoning is correct, then one might expect that the binding of an inhibitor should eliminate the antisymmetric vibrations in the M190A mutant, since the P_1 side-chain of the ligand might restore the missing van der Waals contacts in the S_1 pocket and remove the antisymmetric degree of vibrational freedom. We tested this hypothesis by calculating normal modes for both wild-type and mutant αLP bound to the peptide boronic acid inhibitor, methoxysuccinyl-Ala-Ala-Pro-Ala Boronic acid (data shown in Table 1). As expected, the antisymmetric vibrations are substantially reduced, with the maximum dot product falling by more than 80% for the M190A mutant. Surprisingly, there is also a large reduction in the symmetric vibrations, both in the wild-type and in the mutant, with the maximum dot product falling by 81% and 55%, respectively. While unexpected, this result appears to agree with observations from NMR that dynamics (slow chemical exchange) in the region of the αLP binding site is significantly reduced upon inhibitor binding (Davis & Agard, 1998). Crystallographic *B*-factors in the active site are also reduced somewhat upon binding, with NMA predicting a 20% decrease and experiments showing 12%.

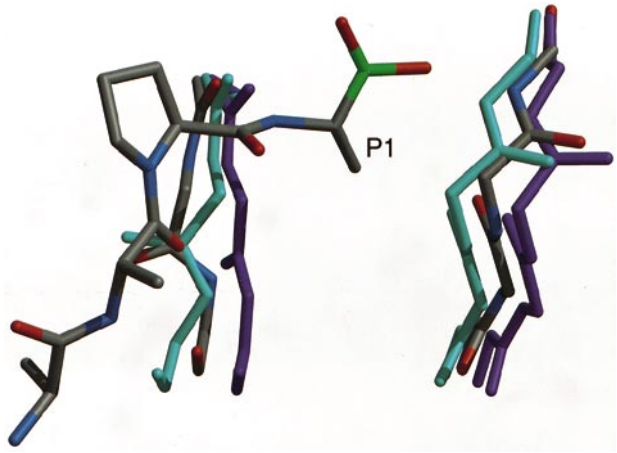

Figure 7. Sample normal modes for wild-type and M190A mutant αLP. Only the region of the S_1 pocket (Figure 1) is shown. The inhibitor is included for reference with previous Figures, but was not present in calculations. The S_1 strands colored by atom type (gray-blue-red) are for the energy-minimized (starting) structure, while the filled-colored strands correspond with the same region of structure projected along a particular normal mode. The wild-type projection (purple) is taken from the lowest frequency mode and is largely symmetric, since opposing walls of the S_1 pocket move in a uniform direction. The mutant projection (cyan) is from the mode of second lowest frequency and is largely antisymmetric: the walls of the pocket close inward, decreasing the pocket volume.

The S_2 pocket

In order to determine whether the effects of the M190A mutation are primarily localized to the S_1 pocket or whether they are more global, we have also analyzed the vibrational motions in the S_2 specificity site. This region provides the binding pocket for residue P_2 of the substrate, and is formed when an external loop (residues 166-179, known as the ''methionine loop'' through homology with chymotrypsin) is pulled in towards the S_1 site upon binding of the ligand (Bone *et al.*, 1987; see Figure 1). Since X-ray crystallographic results suggest the methionine loop is tightly anchored in the bound state but may be allowed more mobility in the unbound state, we expected that its vibrational modes might be significantly reduced by the presence of the inhibitor.

Our analysis confirms this hypothesis. We performed difference-vector calculations similar to those in Figures 5 and 6, using segments of the methionine loop (Tyr171-Gly174) and the S_1 pocket (Ser214-Gly216) for measurements of symmetric and antisymmetric vibrational motion. We found that in the unbound protein, both types of motion have strong components in the low frequency spectrum of the wild-type and mutant enzymes, and that both types of motion are significantly decreased in the inhibitor-bound state (Figure 8 and Table 1). The symmetric and antisymmetric vibrations are reduced by 64% and 82%, respectively, in the wild-type, and by 47% and 61% in the mutant. These results again appear to be consistent with NMR data showing reductions in slow exchange in the methionine loop upon inhibitor binding. An angular analysis, shown in Figure 8, indicates that the optimal axis for symmetric and antisymmetric types of motion is the same in the wild-type and mutant enzymes. The optimal angle value of 60° (illustrated in Figure 5(b) with respect to the αLP structure) is in good agreement with the value of 80° observed for the closing of the methionine loop upon binding of the inhibitor (data not shown). The latter value was determined by comparing the X-ray crystallographic structures of αLP in the free and bound states, and likely represents the axis along which the methionine loop is most flexible in the unbound enzyme.

These results confirm that the M190A mutation has the largest effect at the S_1 pocket and relatively little effect at S_2. While the S_2 vibrational modes have a similar character in the wild-type

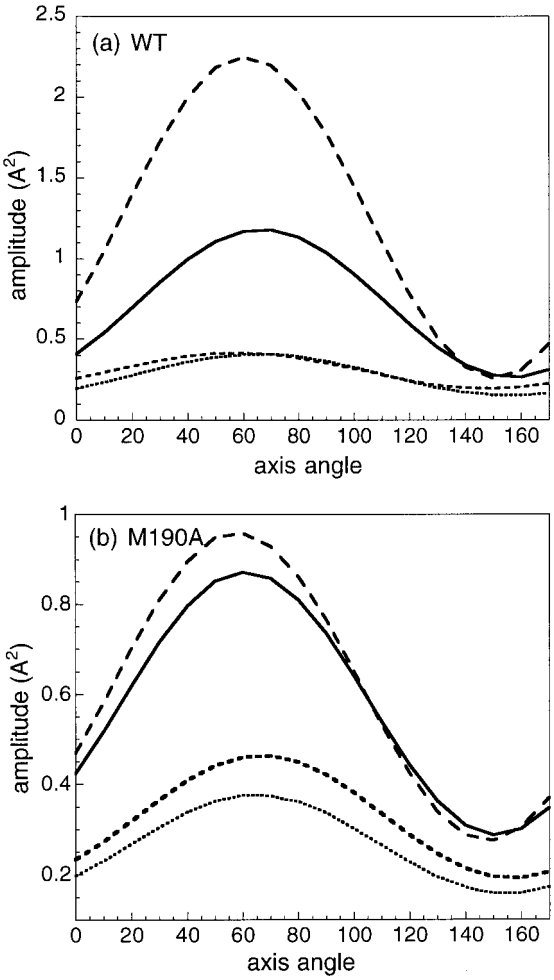

Figure 8. Vibrations of the S_2 pocket. As described in the legend to Figure 6(c) and (d), the cumulative squared dot product after 100 modes (amplitude) is plotted *versus* the angle of vibration. The plots show results for both symmetric (continuous) and antisymmetric (long dashes) motion in the free state, as well as symmetric (short dashes) and antisymmetric (dots) motion in the inhibitor-bound state. The curves show that for both the wild-type (a) and the mutant (b), vibrations occur along the same optimal axis, and that binding of the inhibitor causes significant reductions in both symmetric and antisymmetric motions.

Table 1. α-Lytic protease vibrations at S_1 and S_2

αLP sequence/pocket	Amplitude ratio: symm/anti (unbound)	Reduction in symmetrical vibrations upon binding (%)	Reduction in antisymmetrical vibrations upon binding (%)
Wild-type S_1	11.8	81	12
M190A S_1	1.5	55	80
Wild-type S_2	0.52	64	82
M190A S_2	0.90	47	61

Column 2 is the ratio of symmetric motion to antisymmetric motion, using the cumulative squared dot product (see Figure 6 and Methods) after 100 modes. Calculations correspond with free protein with no inhibitor bound. Columns 3 and 4 are the reductions in the amplitudes of symmetric and antisymmetric motion, respectively, upon binding of the inhibitor. The amplitudes are taken from the cumulative squared dot product after 100 modes.

and the mutant, and are similarly affected by the presence of the inhibitor, at S_1 the effects of the mutation are much more dramatic, significantly altering the character of the vibrations. This result is in agreement with X-ray crystallographic structure analysis (the M190A S_2 pocket is nearly identical with the wild-type) and with crystallographic *B*-factors, which for the S_2 methionine loop changes relatively little upon mutation (Bone *et al*., 1989a).

Discussion

Results from a normal mode analysis indicate that the internal dynamics of αLP undergo a distinct change upon mutation of the single active-site residue Met190. In the wild-type, vibrations are such that the shape of the S_1 specificity pocket tends to be preserved, while in the mutant, vibrations tend to involve expansion and contraction of the pocket. This change in dynamics is one of the directionality of the vibrations, not simply their magnitude: calculated and crystallographic *B*-factors for active-site residues change by only a small amount upon mutation (−16% and −11%, respectively), whereas the amount of vibrational symmetry changes much more dramatically. These results appear to be consistent with the observed specificity profiles for the wild-type and mutant enzymes. While the wild-type αLP is highly specific for the small Ala side-chain at the P_1 position, the mutant has a broadened specificity that allows both small (Ala) and large (Phe) side-chains to be catalyzed at similarly high rates. Our NMA data suggest this difference might result from the predicted increase in structural plasticity in the M190A active site. Thus αLP appears to be an example of an enzyme whose substrate specificity may be at least partially under ''dynamic'' control: the change in specificity upon mutation appears to be driven not only by the change in static structure (although its role is clearly significant), but also by the change in the characteristic vibrations of the active-site residues. It appears that the latter may be important in determining which substrates are allowed access to the S_1 specificity pocket.

αLP is one of a growing number of proteins whose dynamics are known to be important for function. Among the most common dynamic processes are the flexible loop ''lids'' and other similar ''gating'' mechanisms employed to control movement of substrates and products into and out of catalytic sites. Lactate dehydrogenase (White *et al*., 1976), triose phosphate isomerase (Phillips *et al*., 1977), and HIV protease (Miller *et al*., 1989) are examples of enzymes using such mechanisms. In addition, dynamic ''breathing motions'' are important in many proteins for entry of small-molecule ligands into the protein interior. Examples include the binding of oxygen and other small molecules to globins (Case & Karplus, 1979; Henry *et al*., 1983; Gibson *et al*., 1986), the quenching of buried fluorophores by dissolved oxygen (Lakowicz & Weber, 1973), and the exchange of buried amide hydrogen atoms for deuterium atoms in solvated protein crystals (Schoenborn *et al*., 1978; Tuchsen & Ottesen, 1979; Tuchsen *et al*., 1980).

A distinguishing feature of our results is the finding that characteristic motions in the αLP active site can be significantly altered with only a single amino acid substitution. The dramatic effect of the M190A mutation on αLP dynamics suggests that particular vibrational modes may have been optimized not simply to allow access of a substrate into the active site, but also to discriminate between substrates. This level of dynamic control suggests that protein flexibility, in addition to three-dimensional structure, may have been a degree of freedom at the disposal of an evolving enzyme, for use in bringing about a particular catalytic function. The fact that the M190A mutation has a highly localized effect, modulating dynamics only at S_1 rather than at S_2 or other regions, supports the idea that dynamic regulation at important functional sites may be under very fine control.

These results have two possible implications. The first pertains to protein engineering, and is the idea that desired patterns of flexibility might be ''designed into'' a protein by specific mutation, as a means of either selecting or regulating a given function. The second pertains to rational drug design. If dynamics are important for enzyme function, and if the protein regions most responsible for the motion can be identified, they might present a potential target for small-molecule drug binding and inhibition. Such studies are currently being investigated (e.g. Tantillo *et al*., 1994).

Moreover, our work represents a novel use of the NMA method. Whereas most uses of this technique have focused on large collective motions and average properties of proteins, our results are the first to consider as detailed and functionally relevant a property as enzyme specificity. This property can be addressed for two reasons. First, the atoms of the αLP S_1 specificity pocket show elevated and highly symmetric motion in the low-frequency spectrum of the normal modes. Secondly, the dynamics of these S_1-pocket atoms undergo a distinct and measurable change upon mutation of M190. Since NMA is an approximate and ''coarse-grained'' method, such a change might ordinarily be expected to go undetected. However, our results suggest that in cases where a particular mutation can, through the alteration of internal structural constraints in a molecule (such as van der Waals packing), introduce new vibrational degrees of freedom, NMA might prove useful in detecting and quantifying the resulting changes in dynamics. We are currently pursuing methods of increasing our model complexity (using full-atom force fields and including solvent) so that our results can be more rigorously tested.

Methods

Wild-type and M190A mutant α-lytic protease coordinates were taken from the structures referenced 2alp (Fujinaga *et al*., 1985) and 1gbj (Mace *et al*., 1995), respectively, in the Protein Data Bank. The corresponding inhibitor-bound structures, with the inhibitor being MeO-suc-Ala-Ala-Pro-BoroAla, were taken from the structures referenced 1p02 (Bone *et al*., 1989b) and 1gbk (Mace & Agard, 1995). Conjugate gradient minimization was performed using the AMBER 4.1 (Pearlman *et al*., 1995) parameter set and a united-atom representation, in which non-polar hydrogen atoms are absorbed into the adjoining carbon. Minimization was performed *in vacuo* with no cutoff for electrostatics and a dielectric constant equal to four times the inter-atomic distance ($\varepsilon = 4r$). During minimization all non-hydrogen atoms were harmonically constrained to prevent large changes in structure due to bad initial contacts. We performed 100 cycles each of minimization using constraints of 200, 100, 50, 20, 10, and 5 kcal/mol Å^2, followed by roughly 10,000 cycles of unrestrained minimization, until the energy gradient was less than 10^{-4} kcal/mol. This was followed by Newton-Raphson minimization until the gradient fell below 10^{-5} kcal/mol. The final minimized structures had C^{α} rms deviations of 0.80 Å (wild-type) and 0.82 Å (mutant) from their starting crystal structures. The mass-weighted second-derivative matrix H (equation (2)) was calculated using AMBER 4.1 (Pearlman *et al*., 1995), and was diagonalized using standard methods. Matrix dimensions were $3N = 5274$ for the wild-type and $3N = 5259$ for the mutant. Diagonalization required approximately eight hours on an SGI R10,000 processor.

The symmetric and antisymmetric difference vectors were defined by first fitting the two S_1 strands (Figure 1) using two parallel lines. Each of the 25 specificity atoms (see the text) in the S_1 pocket was then assigned a vector with a direction defined by a third line that both intersects the two parallel lines and is perpendicular to them. All vector lengths were arbitrarily chosen to be 1.0 Å. In the full $3N$-dimensional difference vector, all elements are zero except for the 3×25 elements corresponding to the 25 specificity atoms. The dot product is then between the $3N$-element difference vector and a $3N$-element normal mode. The curves in Figure 6(a) and (b) correspond with the cumulative, squared dot product between a difference vector and the 100 lowest frequency normal modes. To test angular dependence, we allowed the atom vectors to rotate collectively about the imaginary axis that passes through the coordinates of a given atom and that runs parallel with the two S_1 strand axes (Figure 5(b)). Dot product calculations were made every 10 deg. using this procedure, and revealed a smooth angular dependence with a maximum dot product observed at 150° relative to the plane connecting the S_1-strand axes (Figure 6(c) and (d)). The difference vector diagram in Figure 5(a) and the dot product calculations in Figure 6(a) and (b) correspond with this maximum. The analyses of the S_2 pocket were performed using a similar procedure.

The amplitude of vibrational motion is calculated using the classical expression:

$$\langle r_j^2 \rangle k_B T \sum_k \frac{|a_{jk}|^2}{\omega_k^2} \qquad (5)$$

where a_{jk} is the magnitude of normal mode k for a single degree of freedom of atom j, k_B is Boltzmann's constant, T is absolute temperature, ω_k is the modal frequency, and $\langle r_j^2 \rangle$ is the atomic mean-squared displacement. Because of its inverse dependence on frequency, the vibrational amplitude receives its dominant contribution from the few lowest frequency normal modes. Figures 6(a) and (b)) show that the cumulative dot-product reaches a plateau after roughly 100 modes.

Acknowledgments

This work was supported by funds from the Howard Hughes Medical Institute. We also wish to thank Dr Ken Dill for numerous useful discussions, and our reviewers for insightful suggestions and comments.

References

Bone, R., Shenvi, A. B., Kettner, C. A. & Agard, D. A. (1987). Serine protease mechanism: structure of an inhibitory complex of α-lytic protease and a tightly bound peptide boronic acid. *Biochemistry*, **26**, 7609-7614.

Bone, R., Silen, J. L. & Agard, D. A. (1989a). Structural plasticity broadens the specificity of an engineered protease. *Nature*, **339**, 191-195.

Bone, R., Frank, D., Kettner, C. A. & Agard, D. A. (1989b). Structural analysis of specificity: α-lytic protease complexes with analogues of reaction intermediates. *Biochemistry*, **28**, 7600-7609.

Bone, R., Fujishige, A., Kettner, C. A. & Agard, D. A. (1991). Structural basis for broad specificity in α-lytic protease mutants. *Biochemistry*, **30**, 10388-10398.

Brayer, G. D., Delbaere, L. T. & James, M. N. G. (1979). Molecular structure of the α-lytic protease from Myxobacter 495 at 2.8 Å resolution. *J. Mol. Biol.* **131**, 743-775.

Brooks, B. & Karplus, M. (1983). Harmonic dynamics of proteins: normal modes and fluctuations in bovine pancreatic trypsin inhibitor. *Proc. Natl Acad. Sci. USA*, **80**, 6571-6575.

Brooks, B. & Karplus, M. (1985). Normal modes for specific motions of macromolecules: application to the hinge-bending mode of lysozyme. *Proc. Natl Acad. Sci. USA*, **82**, 4995-4999.

Burling, F. T., Weis, W. I., Flaherty, K. M. & Brünger, A. T. (1996). Direct observation of protein solvation and discrete disorder with experimental crystallographic phases. *Science*, **271**, 72-77.

Case, D. A. (1994). Normal mode analysis of protein dynamics. *Curr. Opin. Struct. Biol.* **4**, 285-290.

Case, D. A. & Karplus, M. (1979). Dynamics of ligand binding to heme proteins. *J. Mol. Biol.* **132**, 343-368.

Daggett, V. & Levitt, M. (1993). Realistic simulations of native-protein dynamics in solution and beyond. *Annu. Rev. Biophys. Biomol. Struct.* **22**, 353-380.

Davis, J. H. & Agard, D. A. (1998). Relationship between enzyme specificity and the backbone dynamics of free and inhibited α-lytic protease. *Biochemistry*, **37**, 7696-7707.

Diamond, R. (1990). On the use of normal modes in thermal parameter refinement: theory and application to the bovine pancreatic trypsin inhibitor. *Acta Crystallog. sect. A*, **46**, 425-435.

Durand, P., Trinquier, G. & Sanejouand, Y. (1994). A new approach for determining low-frequency

normal modes in macromolecules. *Biopolymers*, **34**, 759-771.

Ech-Cherif, El-Kettani M. A. & Durup, J. (1992). Theoretical determination of conformational paths in citrate synthase. *Biopolymers*, **32**, 561-574.

Ferrin, T. E., Huang, C. C., Jarvis, L. E. & Langridge, R. (1988). The MIDAS display system. *J. Mol Graph.* **6**, 13-27.

Fujinaga, M., Delbaere, L. T. J., Brayer, G. D. & James, M. N. G. (1985). Refined structure of α-lytic protease at 1.7 Å resolution. Analysis of hydrogen bonding and solvent structure. *J. Mol. Biol.* **183**, 479-502.

Gibrat, J. & Go, N. (1990). Normal mode analysis of human lysozyme: study of the relative motion of the two domains and characterization of the harmonic motion. *Proteins: Struct. Funct. Genet.* **8**, 258-279.

Gibson, Q. H., Olson, J. S., McKinnie, R. E. & Rohlfs, R. J. (1986). A kinetic description of ligand binding to sperm whale myoglobin. *J. Biol. Chem.* **261**, 10228-10239.

Go, N., Noguti, T. & Nishikawa, T. (1983). Dynamics of a small globular protein in terms of low-frequency vibrational modes. *Proc. Natl Acad. Sci. USA*, **80**, 3696-3700.

Hao, M. & Harvey, S. C. (1992). Analyzing the normal mode dynamics of macromolecules by the component synthesis method. *Biopolymers*, **32**, 1393-1405.

Hao, M. & Scheraga, H. A. (1994). Analyzing the normal mode dynamics of macromolecules by the component synthesis method: residue clustering and multiple-component approach. *Biopolymers*, **34**, 321-335.

Harrison, W. (1984). Variational calculation of the normal modes of a large macromolecule: methods and some initial results. *Biopolymers*, **23**, 2943-2949.

Hayward, S., Kitao, A. & Go, N. (1994). Harmonic and anharmonic aspects in the dynamics of BPTI: a normal mode analysis and principal component analysis. *Protein Sci.* **3**, 936-943.

Hayward, S., Kitao, A. & Go, N. (1995). Harmonicity and anharmonicity in protein dynamics: a normal mode analysis and principal component analysis. *Proteins: Struct. Funct. Genet.* **23**, 177-186.

Henry, E. R., Sommer, J. H., Hofrichter, J. & Eaton, W. A. (1983). Geminate recombination of carbon monoxide to myoglobin. *J. Mol. Biol.* **166**, 443-451.

Horiuchi, T. & Go, N. (1991). Projection of Monte Carlo and molecular dynamics trajectories onto the normal mode axes. *Proteins: Struct. Funct. Genet.* **10**, 106-116.

Huang, C. C., Pettersen, E. F., Klein, T. E., Ferrin, T. E. & Langridge, R. (1991). Conic: a fast renderer for space-filling molecules with shadows. *J. Mol. Graph.* **9**, 230-236.

Ichiye, T. & Karplus, M. (1991). Collective motions in proteins: a covariance analysis of atomic fluctuations in molecular dynamics and normal mode simulations. *Proteins: Struct. Funct. Genet.* **11**, 205-217.

James, M. N., Delbaere, L. T. & Brayer, G. D. (1978). Amino acid sequence alignment of bacterial and mammalian pancreatic serine proteases based on topological equivalences. *Can. J. Biochem.* **56**, 396-402.

Karplus, M. & Kushick, J. N. (1981). Method for estimating the configurational entropy of macromolecules. *Macromolecules*, **14**, 325-332.

Kidera, A. & Go, N. (1992). Normal mode refinement: crystallographic refinement of protein dynamics structure. I. Theory and Test by simulated diffraction data. *J. Mol. Biol.* **225**, 457-475.

Kidera, A., Inaka, K., Matsushima, M. & Go, N. (1992). Normal mode refinement: crystallographic refinement of protein dynamics structure. II. Application to human lysozyme. *J. Mol. Biol.* **225**, 477-486.

Lakowicz, J. R. & Weber, G. (1973). Quenching of fluorescence by oxygen. A probe for structural fluctuations in macromolecules. *Biochemistry*, **12**, 4161-4170.

Levitt, M., Sander, C. & Stern, P. S. (1985). Protein normal-mode dynamics: trypsin inhibitor, crambin, ribonuclease and lysozyme. *J. Mol. Biol.* **181**, 423-447.

Levy, R. M., Karplus, M., Kushick, J. & Perahia, D. (1984). Evaluation of the configurational entropy for proteins: application to molecular dynamics simulations of an α-helix. *Macromolecules*, **17**, 1370-1374.

Mace, J. E. & Agard, D. A. (1995). Kinetic and structural characterization of mutations of glycine 216 in α-lytic protease: a new target for engineering substrate specificity. *J. Mol. Biol.* **254**, 720-736.

Mace, J. E., Wilk, B. J. & Agard, D. A. (1995). Functional linkage between the active site of α-lytic protease and distant regions of structure: scanning alanine mutagenesis of a surface loop affects activity and substrate specificity. *J. Mol. Biol.* **251**, 116-134.

Marques, O. & Sanejouand, Y. (1995). Hinge-bending motion in citrate synthase arising from normal mode calculations. *Proteins: Struct. Funct. Genet.* **23**, 557-560.

Miller, M., Schneider, J., Sathyanarayana, B. K., Toth, M. V., Marshall, G. R., Clawson, L., Selk, L., Kent, S. B. & Wlodawer, A. (1989). Structure of a complex of synthetic HIV-1 protease with a substrate-based inhibitor at 2.3 Å resolution. *Science*, **246**, 1149-1152.

Mouawad, L. & Perahia, D. (1993). Diagonalization in a mixed basis: a method to compute low-frequency normal modes for large macromolecules. *Biopolymers*, **33**, 599-611.

Mouawad, L. & Perahia, D. (1996). Motions in hemoglobin studied by normal mode analysis and energy minimization: evidence for the existence of tertiary T-like, quaternary R-like intermediate structures. *J. Mol. Biol.* **258**, 393-410.

Pauling, L. (1948). Nature of forces between large molecules of biological interest. *Nature*, **161**, 707-709.

Pearlman, D. A., Case, D. A., Caldwell, J. W., Wilson, S. R., Cheatham, T. E., Ferguson, D. M., Seibel, G. L., Singh, U. C., Weiner, P. K. & Kollman, P. A. (1995). *AMBER 4.1*, University of California, San Francisco.

Phillips, D. C., Rivers, P. S., Sternberg, M. J. E., Thornton, J. M. & Wilson, I. A. (1977). An analysis of the three-dimensional structure of chicken triose phosphate isomerase. *Trans. Biochem. Soc.* **5**, 642-647.

Rader, S. D. & Agard, D. A. (1997). Conformational substates in enzyme mechanism: the 120 K structure of α-lytic protease at 1.5 Å resolution. *Protein Sci.* **6**, 1375-1386.

Sanejouand, Y. H. (1996). Normal-mode analysis suggests important flexibility between the two N-terminal domains of CD4 and supports the hypothesis of a conformational change in CD4 upon HIV binding. *Protein Eng.* **9**, 671-677.

Sauter, N. K., Mau, T., Rader, S. D. & Agard, D. A. (1998). The structure of α-lytic protease complexed with its pro region. *Nature Struct. Biol.* **5**, 945-950.

Schechter, I. & Berger, A. (1967). On the size of the active site in proteases. *Biochem. Biophys. Res. Commun.* **27**, 157-162.

Schoenborn, B. P., Hanson, J. C., Darling, G. D. & Norvell, J. C. (1978). Real space refinement of neutron diffraction data from carbon monoxide sperm whale myoglobin. *Acta. Crystallog. sect. A*, **34**, 65.

Tantillo, C., Ding, J., Jacobo-Molina, A., Nanni, R. G., Boyer, P. L., Hughes, S. H., Pauwels, R., Andries, K., Janssen, P. A. J. & Arnold, E. (1994). Locations of anti-AIDS drug binding sites and resistance mutations in the three-dimensional structure of HIV-1 reverse transcriptase. *J. Mol. Biol.* **243**, 369-387.

Teeter, M. M. & Case, D. A. (1990). Harmonic and quasiharmonic descriptions of crambin. *J. Phys. Chem.* **94**, 8091-8097.

Thomas, A., Roux, B. & Smith, J. C. (1993). Computer simulations of the flexibility of a series of synthetic cyclic peptide analogues. *Biopolymers*, **33**, 1249-1270.

Tidor, B. & Karplus, M. (1993). The contribution of cross-links to protein stability: a normal mode analysis of the configurational entropy of the native state. *Proteins: Stuct. Funct. Genet.* **15**, 71-79.

Tiron, M. M. & ben-Avraham, D. (1993). Normal mode analysis of G-actin. *J. Mol. Biol.* **230**, 186-195.

Tuchsen, E. & Ottesen, M. (1979). A simple hydrogen exchange method for cross-linked protein crystals. *Carlsberg Res. Commun.* **44**, 1-10.

Tuchsen, E., Hvidt, A. & Ottesen, M. (1980). Enzymes immobilized as crystals. Hydrogen isotope exchange of crystalline lysozyme. *Biochimie*, **62**, 563-566.

Wallace, R. A., Abraham, N. K. & Niemann, C. (1963). Interaction of aromatic compounds with α-chymotrypsin. *Biochemistry*, **2**, 824-836.

White, J., Hackert, M. L., Buehner, M., Adams, M. J., Ford, G. C., Lentz, P. J., Smiley, I. E., Steindel, S. J. & Rossmann, M. G. (1976). A comparison of the structures of apo dogfish M4 lactate dehydrogenase and its ternary complexes. *J. Mol. Biol.* **102**, 759-779.

Edited by P. E. Wright

(Received 26 June 1998; received in revised form 25 November 1998; accepted 25 November 1998)